Vibration Reduction in an Unbalanced Rotor System Using Nonlinear Energy Sinks with Varying Stiffness

Harikrishnan Venugopal(✉), Kevin Dekemele, and Mia Loccufier

Department of Electromechanical Systems and Metal Engineering, Ghent University, Tech Lane Ghent Science Park- Campus A 125, 9052 Ghent, Belgium
{harikrishnan.venugopal,kevin.dekemele,mia.loccufier}@ugent.be

Abstract. The study of dynamics of rotating machinery has risen to be of great importance in recent decades, with the industry vying for higher operating speeds, higher loads, and lower weight. This trend tends to place the system in the vicinity of its critical speeds, limiting its operational potential, and the traditional approach to reduce vibrations is to attach a tuned mass damper to the system. However, these are tuned based on 1:1 resonance of the system and fail to work effectively otherwise. Accordingly, recent developments have seen the use of the Nonlinear Energy Sink (NES) as their substitute, providing a more robust means of vibration mitigation, by being functional for a broad range of frequencies. In this paper, a passive vibration absorber with nonlinear stiffness is attached to a simple Jeffcott rotor. A speed-dependent force due to mass eccentricity is used here, as is common in rotordynamic systems. The conventional hardening (cubic) stiffness and a newly introduced softening stiffness are studied for their feasibility and compared against each other based on their behaviour and performance. The system's frequency response is obtained using first-order harmonic balancing and the stability of the solution branches is studied using the multiple time-scales method. Furthermore, a parametric study of the response behaviour and NES performance for various stiffness characteristics is presented. With these methods, one can effectively prove the feasibility of using NESs for vibration mitigation in rotor systems.

Keywords: Nonlinear Energy Sink · Harmonic balancing · Jeffcott rotor · Tuning Methodology · Nonlinear Stiffness

1 Introduction

The field of rotordynamics has seen a burst of development in the recent decades due to general industry trends towards lower weight, higher power density and higher operating speeds. While understandable in terms of increasing productivity, these developments worsen the issues regarding vibration and stability of rotor systems. In this regard, it may not always be possible to restrict the rotational speed of the system within its first critical speed, and a stable operating speed would need to be obtained by running through one or more critical speeds [1, 2]. Accordingly, it becomes a priority to mitigate the vibrations of the system at these resonances.

F. Chu and Z. Qin (Eds.): IFToMM 2023, MMS 139, pp. 358–373, 2024.
https://doi.org/10.1007/978-3-031-40455-9_30

Nonlinear Energy Sink(s) (NES) come across as a potential solution. They are passive vibration control devices with nonlinear stiffness or damping characteristics, connected to a host system under consideration. NESs are becoming increasingly popular due to their capability to tackle multiple resonant frequencies and act as a broadband vibration absorber [3]. The NES is incapable of completely suppressing the host system resonant response like the TMD but it is more effective in the vicinity of the resonance. Furthermore, NES can perform better in case of perturbations in the host system parameters, in comparison to the traditional Tuned Mass Damper(s) (TMD) [4]. It should be noted that the design of the NES is more challenging than for a TMD, as here the host system's response is dependent on the forcing magnitude and can have detached bifurcations and regions of quasi-periodic, 'beating' oscillations [3, 5].

Recent research has shown that NES is perfectly capable of tackling a myriad of issues in rotordynamics. Ghasem et.al. [6] used NES to deal with the problem of rotor-stator contact in an unbalanced Jeffcot rotor. Here, a Jeffcot rotor mounted on journal bearings is subjected to rotor-stator contact force and mass unbalance forces, and thereafter, different configurations of NESs and TMDs are evaluated. The suitability of NES for a more representative primary system with a flexible/rigid rotor with flexible blades is investigated by Bab et al. [7]. Apart from rotor-stator interactions, the mass unbalance force has also been studied by Hongliang et al. [8] using magnetic NES, with both cubic and linear stiffness. The results point favourably towards implementing higher nonlinearity, however its effects on system stability are yet to be observed. As for realizing various nonlinearities, a nonlinear stiffness is modelled in [3] by running the linear spring over a nonlinear path. A similar idea for obtaining custom nonlinear forces is also expounded in [9]. A summary of the former technique is presented in the appendix.

In the current study, an NES with nonlinear stiffness is attached to a rotor system with mass unbalance forcing. Two different types of nonlinearities are considered, namely hardening and softening [10]. A parametric study is also conducted to explain the bifurcating and quasi-periodic behaviour of the responses. Finally, both stiffness types are compared on their ability to reduce peak response of the primary system.

2 Theoretical Formulation

A representation of a 4-degree of freedom Jeffcott rotor is shown in Fig. 1 above. The rotor rotates with speed ω, and has polar moment of inertia I_p, diametrical moment of inertia I_d and a mass m concentrated at a distance e from the axis of its rotation. This eccentricity creates a centrifugal force which is dependent on the rotational speed of the system. The rigid rotor shaft is connected to two bearings A and B, each possessing a stiffness and damping in x and y direction. The rotor is located at a distance h from bearing A. Apart from the linear motion in the x and y coordinates, the rotor can also have rotatory motion in φ and θ axes. The equations of motion for this system is as follows:

$$m\ddot{y} + k_{Ay}(y + h\varphi) + k_{By}(y - (L-h)\varphi) + c_{Ay}(\dot{y} + h\dot{\varphi}) + c_{By}(\dot{y} - (L-h)\dot{\varphi}) = me\omega^2 sin(\omega t) \tag{1}$$

$$m\ddot{x} + k_{Ax}(x - h\theta) + k_{Bx}(x + (L-h)\theta) + c_{Ax}\left(\dot{x} - h\dot{\theta}\right) + c_{Bx}\left(\dot{x} + (L-h)\dot{\theta}\right) = me\omega^2 \cos(\omega t) \tag{2}$$

$$I_d\ddot{\theta} + I_p\omega\dot{\varphi} - hk_{Ax}(x - h\theta) + (L-h)k_{Bx}(x + (L-h)\theta) - hc_{Ax}\left(\dot{x} - h\dot{\theta}\right) + (L-h)c_{Bx} \left(\dot{x} + (L-h)\dot{\theta}\right) = 0 \tag{3}$$

$$I_d\ddot{\varphi} - I_p\omega\dot{\theta} + hk_{Ay}(y + h\varphi) - (L-h)k_{By}(y - (L-h)\varphi) + hc_{Ay}(\dot{y} + h\dot{\varphi}) - (L-h)c_{By}(\dot{y} - (L-h)\dot{\varphi}) = 0 \tag{4}$$

In many cases, it is reasonable to assume that the system is symmetric; both in terms of its bearings' properties (equal stiffness and damping) and the location of the rotor ($h = L/2$). This decouples the dynamic equations Eqs. (1) and (2). Furthermore, this makes it also reasonable to neglect Eqs. (3) and (4) as the force due to eccentricity doesn't excite the respective resonances in θ and φ coordinates. Hereby we obtain a simplified system as shown in Fig. 2 below. Note that a NES with mass m_{na}, nonlinear stiffness (Fig. 3) k_{na}, and linear damping c_{na} is shown attached to the primary system.

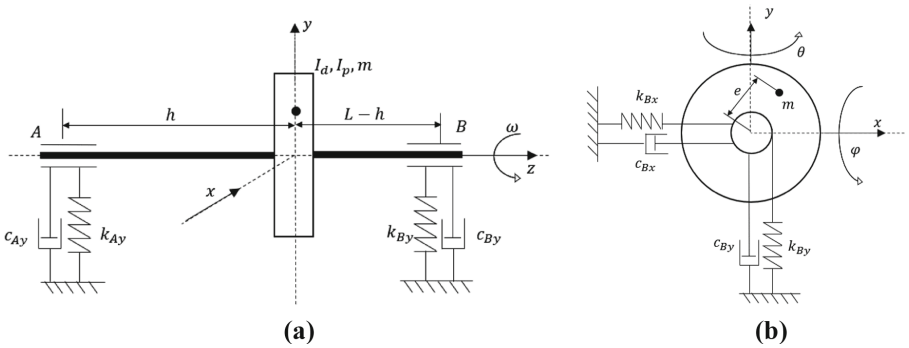

Fig. 1. Representation of the 4-DoF Jeffcot Rotor model, with front view (a) and side view (b)

The dynamics of the simplified Jeffcott rotor with the NES can be expressed by the following equations:

$$m\ddot{x} + c\dot{x} + kx + c_{na}(\dot{x} - \dot{x}_{na}) + k_{na}F(x - x_{na}) = me\omega^2 cos(\omega t) \tag{5}$$

$$m_{na}\ddot{x}_{na} + c_{na}(\dot{x}_{na} - \dot{x}) + k_{na}F(x_{na} - x) = 0 \tag{6}$$

where,

$$F(x_{na} - x) = (x_{na} - x)^3, \text{ for hardening stiffness} \tag{7}$$

$$F(x_{na} - x) = arctan(k_s(x_{na} - x)), \text{ for softening stiffness.} \tag{8}$$

Note that the decoupled state of the Eqs. (1) and (2) allows us to treat each coordinate separately. In this case, they share the same natural frequency at $\omega_{1,2} = \sqrt{k/m}$, and hence the same tuned NES can be used in both coordinates. Realizations of different.

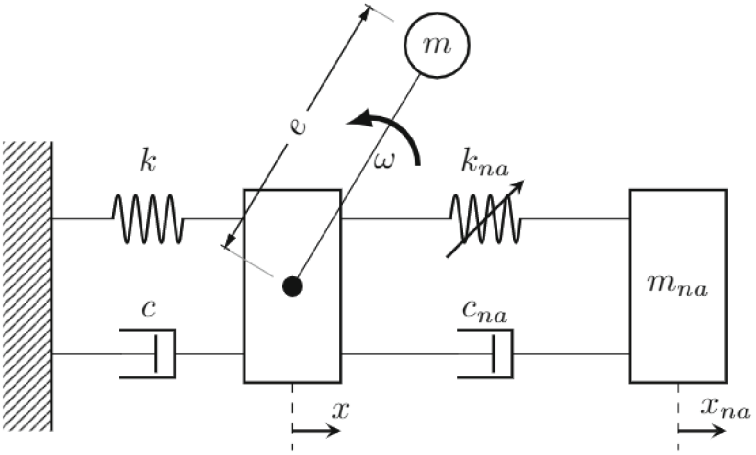

Fig. 2. Representation of the simplified Jeffcott rotor with NES attachment

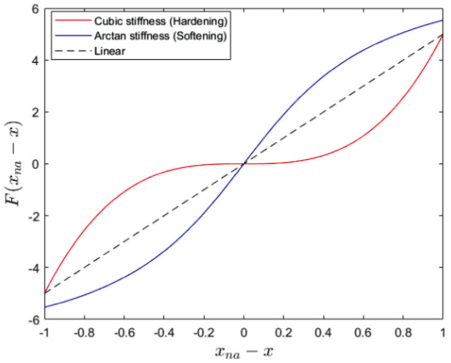

Fig. 3. Comparison of stiffness functions

2.1 Application of Harmonic Balancing

The principle of Harmonic Balancing (HB) rests on the idea that a periodic solution of an ordinary differential equation can be approximated by its truncated Fourier series. While linear ordinary differential equations require only a single harmonic to represent their solution, nonlinear ones lead to solutions with multiple dominant harmonics. An in-depth explanation of the method is provided in [11]. Examples of its implementation for both transient and forced systems are also seen in [3, 12, 13]. Eqs. (5) and (6) are modified as follows:

$$\ddot{x} + \mu\omega_0\xi\dot{x} + \omega_0^2 x + \mu\ddot{x}_{na} = \mu\omega^2 P cos(\omega t) \tag{9}$$

$$\mu\ddot{x}_{na} + \mu\omega_0\xi_{na}(\dot{x}_{na} - \dot{x}) + \mu\omega_0^2\gamma F(x_{na} - x) = 0 \tag{10}$$

where,

$$\mu\omega_0\xi m = c \qquad m\omega_0^2 = k$$
$$\omega_0\xi_{na}m_{na} = c_{na} \quad m\mu = m_{na}$$
$$m_{na}\gamma\omega_0^2 = k_{na} \qquad \mu P = e$$

Here the solution of the equations via HB is represented as a first order harmonic. Thus we introduce the following expression:

$$\frac{\dot{x}}{i\omega} + x = 2A(t)e^{i\omega t} \tag{11}$$

$$\frac{\dot{z}}{i\omega} + z = 2B(t)e^{i\omega t} \tag{12}$$

Both *A* and *B* are time dependent complex variables containing the amplitude and phase information of the response and $z = x_{na} - x$. The time dependence is not shown further explicitly. These variables can be used to describe a slow moving envelope of vibration [14]. A major advantage of complexification is that by separating the oscillations term ($e^{i\omega t}$) and the envelope (A and B), the second-order equations of motion can be modified to a first-order equations for the envelope motion whereafter the fixed points and their stability can be studied with ease. From Eqs. (11) and (12) we get:

$$\frac{\dot{x}}{i\omega} + x + \left(\frac{\dot{x}}{i\omega} + x\right)^* = 2(Ae^{i\omega t} + A^*e^{-i\omega t}) \Rightarrow x = Ae^{i\omega t} + A^*e^{-i\omega t} \tag{13}$$

$$\frac{\dot{x}}{i\omega} + x - \left(\frac{\dot{x}}{i\omega} + x\right)^* = 2(Ae^{i\omega t} - A^*e^{-i\omega t}) \Rightarrow \dot{x} = i\omega(Ae^{i\omega t} - A^*e^{-i\omega t}) \tag{14}$$

Similarly,

$$z = x_{na} - x = Be^{i\omega t} + B^*e^{-i\omega t} \tag{15}$$

$$\dot{z} = i\omega(Be^{i\omega t} - B^*e^{-i\omega t}) \tag{16}$$

The superscript * represents complex conjugate. Differentiating Eq. (11) we get:

$$\frac{\ddot{x}}{i\omega} + \dot{x} = 2\dot{A}e^{i\omega t} + 2i\omega Ae^{i\omega t} \tag{17}$$

Substituting Eqs. (14) and (13) in Eq. (17) we get the following relation:

$$\ddot{x} + \omega^2 x = 2i\omega\dot{A}e^{i\omega t} \tag{18}$$

Similarly,

$$\ddot{z} + \omega^2 z = 2i\omega\dot{B}e^{i\omega t} \tag{19a}$$

For first order HB, the Fourier series coefficient of the first harmonic of the nonlinear stiffness function $F(z)$ is also calculated as follows:

$$F_1(z) = B.f(B, B^*) = \frac{\omega}{2\pi} \int_0^{\frac{2\pi}{\omega}} k_{na} F\left(B, B^*\right) e^{-i\omega t} dt \tag{19b}$$

$$f\left(B, B^*\right) = 3B.B^* \text{ Equation for hardening stiffness} \tag{20}$$

$$f\left(B, B^*\right) = \frac{\sqrt{4BB^*k_s^2 + 1} - 1}{2BB^*k_s} \text{ Equation for softening stiffness} \tag{21}$$

Substituting Eqs. (11)–(19b) in Eqs. (9) and (10) we get:

$$2i\omega\dot{A} + (\omega_0^2 - \omega^2)A + i\mu\omega_0\omega\xi B + \mu(2\dot{A}i\omega - \omega^2 A + 2\dot{B}i\omega - \omega^2 B) = \frac{\mu\omega^2 P}{2} \tag{22}$$

$$2i\dot{B}\omega - \omega^2 B + 2i\omega\dot{A} - \omega^2 A + i\xi_{na}\omega_0\omega B + \omega_0^2\gamma B f(B, B^*) = 0 \tag{23}$$

In order to find the response at the state of steady oscillation, we assume $\dot{A} = \dot{B} = 0$. Thus, the above equations become:

$$\sigma A + i\xi\sqrt{X}A - XA - XB = PX/2 \tag{24}$$

$$i\xi_{na}\sqrt{X}B - XA - XB + \gamma f(B, B^*) = 0 \tag{25}$$

where,

$$X = \frac{\omega^2}{\omega_0^2} \text{ and } 1 - X = \mu\sigma \tag{26}$$

Squaring the real and imaginary parts of Eq. (25) respectively we obtain:

$$X^2A^2 = B^2\left(\xi_{na}^2 X + \left(\gamma f\left(B, B^*\right) - X\right)^2\right) \tag{27}$$

Multiplying Eq. (24) by X and substituting in Eq. (25) for XA we get:

$$\begin{aligned} i\left(\sigma\xi_{na}\sqrt{X} + \xi\sqrt{X}\left(\gamma f\left(B, B^*\right) - X\right) - X\xi_{na}\sqrt{X}\right)B \\ + \left((\sigma - X)\left(\gamma f\left(B, B^*\right) - X\right) - \xi\xi_{na}X - X^2\right)B = \frac{PX^2}{2} \end{aligned} \tag{28}$$

Squaring the real and imaginary part of Eq. (28) ,we get:

$$\begin{aligned} \left(\left((X - \sigma)\left(\gamma f\left(B, B^*\right) - X\right) + \xi\xi_{na}X + X^2\right)^2 + X\left(\xi_{na}(X - \sigma) + \xi\left(X - \gamma f\left(B, B^*\right)\right)\right)^2\right)B^2 \\ = \frac{P^2X^4}{4} \end{aligned} \tag{29}$$

Since the variables A and B are complex in nature, they can be expressed in their polar form as follows:

$$A = \frac{a}{2}e^{i\alpha} \quad B = \frac{b}{2}e^{i\beta} \tag{30}$$

Substituting Eq. (30) in Eqs. (27) and (29) we get:

$$X^2a^2 = b^2\left(\xi_{na}^2X + (\gamma f(b) - X)^2\right) \tag{31}$$

$$\left(\left((X-\sigma)(\gamma f(b) - X) + \xi\xi_{na}X + X^2\right)^2 + X(\xi_{na}(X-\sigma) + \xi(X - \gamma f(b)))^2\right)b^2 = P^2X^4 \tag{32}$$

For a given value of X, Eq. (32) can be solved for b. Equation (31) is the Slow Invariant Manifold (SIM) relating a and b. It should be noted that the relation is also dependent on the frequency ratio X and forcing P. Dividing Eq. (31) by Eq. (32) we get the expression for the nonlinear frequency response of the primary system:

$$\frac{a}{P} = \sqrt{\frac{X^2\left(\xi_{na}^2X + (\gamma f(b) - X)^2\right)}{D(X,b)}} \tag{33}$$

where,

$$D(X,b) = \left(\left((X-\sigma)(\gamma f(b) - X) + \xi\xi_{na}X + X^2\right)^2 + X(\xi_{na}(X-\sigma) + \xi(X - \gamma f(b)))^2\right)$$

2.2 Estimation of Solution Stability

From the equations above we have found the fixed points a and b of the system by assuming steady state. To characterize the stability of these points, we use the multiple time-scales theory [3, 12, 13]. Here we interpret the total time spent as the sum of two time scales, one moving across the time domain faster than the other:

$$\tau_1 = \omega_0 t \quad \tau_2 = \mu\omega_0 t \tag{34}$$

Here $\tau_1 \gg \tau_2$, implying that τ_1 is the faster time scale. The main advantage of this method becomes evident, as we are more interested in the long-term evolution of the response envelope. The time derivative is modified as shown below:

$$\frac{d}{dt} = \omega_0\frac{\partial}{\partial\tau_1} + \mu\omega_0\frac{\partial}{\partial\tau_2} \tag{35}$$

Substituting the modified derivative into Eqs. (22) and (23) and reorganizing the terms according to the power of μ we get:

$$\mu^0: \quad 2i\omega_0\omega\frac{\partial A}{\partial\tau_1} = 0 \tag{36a}$$

$$2i\omega_0\omega\frac{\partial B}{\partial\tau_1} - \omega^2A - \omega^2B + i\omega_0\omega\xi_{na}B + \omega_0^2\gamma B.f(B,B^*) = 0 \tag{36b}$$

$$\mu^1: \quad 2i\omega_0\omega\frac{\partial A}{\partial \tau_2} + \omega_0^2\sigma A + i\omega_0\omega\xi B - \omega^2 A - \omega^2 B = \omega^2\frac{P}{2} \tag{37a}$$

$$2i\omega_0\omega\frac{\partial B}{\partial \tau_2} + 2i\omega_0\omega\frac{\partial A}{\partial \tau_2} = 0 \tag{37b}$$

Rewriting the Eq. (36b) in terms of X we get:

$$\frac{\partial B}{\partial \tau_1} = \Gamma\left(A, B, B^*, X\right) = \frac{1}{2\sqrt{X}}\left(iXB + iXA - i\omega_0^2\gamma Bf\left(B, B^*\right) - \xi_{na}\sqrt{X}B\right) \tag{38}$$

Equation (38) is linearized at the fixed points previously found:

$$B = B_{eq} + \Delta B \tag{39a}$$

$$\frac{\partial B}{\partial \tau_1} = 0 + \Delta\left(\frac{\partial B}{\partial \tau_1}\right) \tag{39b}$$

Combining the relation from Eq. (38) and expanding, we get:

$$\Rightarrow \Delta\Gamma = \left(\frac{\partial \Gamma}{\partial B}\right)_{B=B_{eq}} \Delta B + \left(\frac{\partial \Gamma}{\partial B^*}\right)_{B=B_{eq}} \Delta B^* \tag{40}$$

$$a_{11} = a_{22}^* = \left(\frac{\partial \Gamma}{\partial B}\right)_{B=B_{eq}} \qquad a_{12} = a_{21}^* = \left(\frac{\partial \Gamma}{\partial B^*}\right)_{B=B_{eq}} \tag{41}$$

$$\begin{bmatrix} \Delta\Gamma \\ \Delta\Gamma^* \end{bmatrix} = \begin{bmatrix} a_{11} & a_{12} \\ a_{21} & a_{22} \end{bmatrix} \begin{bmatrix} \Delta B \\ \Delta B^* \end{bmatrix} \tag{42}$$

The Eq. (42) is the linearized state equation of the system and the eigenvalues of the Jacobian matrix dictate the stability. Positive real eigenvalues indicate instability of the chosen fixed point.

3 Parametric Analysis on Response Behaviour

In this analysis, a parametric study is conducted by varying the stiffness parameters, keeping other parameters constant. For hardening stiffness, this means changing the factor γ and for softening stiffness both k_s and γ are to be varied (see Eqs. (5)–(8)).

The system is analysed close to its resonance, by varying frequency ratio (ω/ω_0) from 0.9 to 1.1. Firstly, a numerical simulation of the system is performed by using the Runge-Kutta (RK) method, implemented by the ODE 45 function in MATLAB. The envelope of time signal is obtained, and the upper and lower values of the envelope are plotted in blue and orange circles respectively (Fig. 4). Thereafter, the solution from the HB is compared with the numerical solution and with a primary system without an NES. Stability of the solution branches are also evaluated. Stable branches are shown in black and the unstable ones are shown in red.

Table 1. Parameter values for primary system with hardening NES.

Parameter	Value
ξ_{na}	0.25
ξ	1
γ	1–400
μ	0.01
ω_0[rad/s]	1
e[m]	0.001

3.1 Primary system with hardening NES

The parameter values for the primary system with hardening NES are given in Table 1 below. Note that the dimensionless parameters of Eq. (9) and (10) can be used as inputs, so that a general class of system can be defined.

In Fig. 4, we can see the evaluation of the primary system frequency response w.r.t the stiffness factor γ. It is observed that for all γ the numerical simulations agree closely with the HB-solutions, except in the regions of HB-unstable. Increasing this constant increases the degree of nonlinearity of the stiffness force. This means that at higher γ the displacement will get to traverse regions of higher nonlinearity (i.e. Here, as γ increases, the response at the primary system's resonance is indeed being suppressed, but with the introduction of certain unconventional behaviour. At $\gamma = 55$ (Fig. 4b and c), we see regions of instability arise near the resonance. However, it should be noted that the stability here only means that the envelope magnitude is not steady as assumed ($\dot{A} = \dot{B} = 0$); as from simulations it is seen that the response resembles that of a quasi-periodic response (Fig. 8). This phenomenon is also referred to as Neimark-Sacker bifurcation [15]. This is also shown in the plot, as the upper and lower envelope values don't coincide in this region.

At $\gamma = 185$ (Fig. 4d), we see the inception of a bifurcation, detached from the main curve. This is referred to as an Isolated Resonance Curve (IRC), and is often considered to be disadvantageous for NES tuning. This is because of the possibility that the response can fall into to these resonance curves when started at certain initial conditions.

As γ increases, the IRCs become larger in size and merge with the main curve at $\gamma = 200$ (Fig. 4e). At this point we can see how the numerical solution (with zero initial displacement and velocity) follows the now attached part of the IRC. As γ increases further, this results in the formation of two separate bifurcations (Fig. 4f), one on either side of the resonance peak. Additionally, the peak of the almost-attached IRC, becomes the new response peak. The two bifurcations diverge from each other as γ increases.

It should be noted that increasing the damping via ξ_{na} or ξ, only raises the lower limit of values of γ where a particular phenomenon is found. The behavior remains just the same.

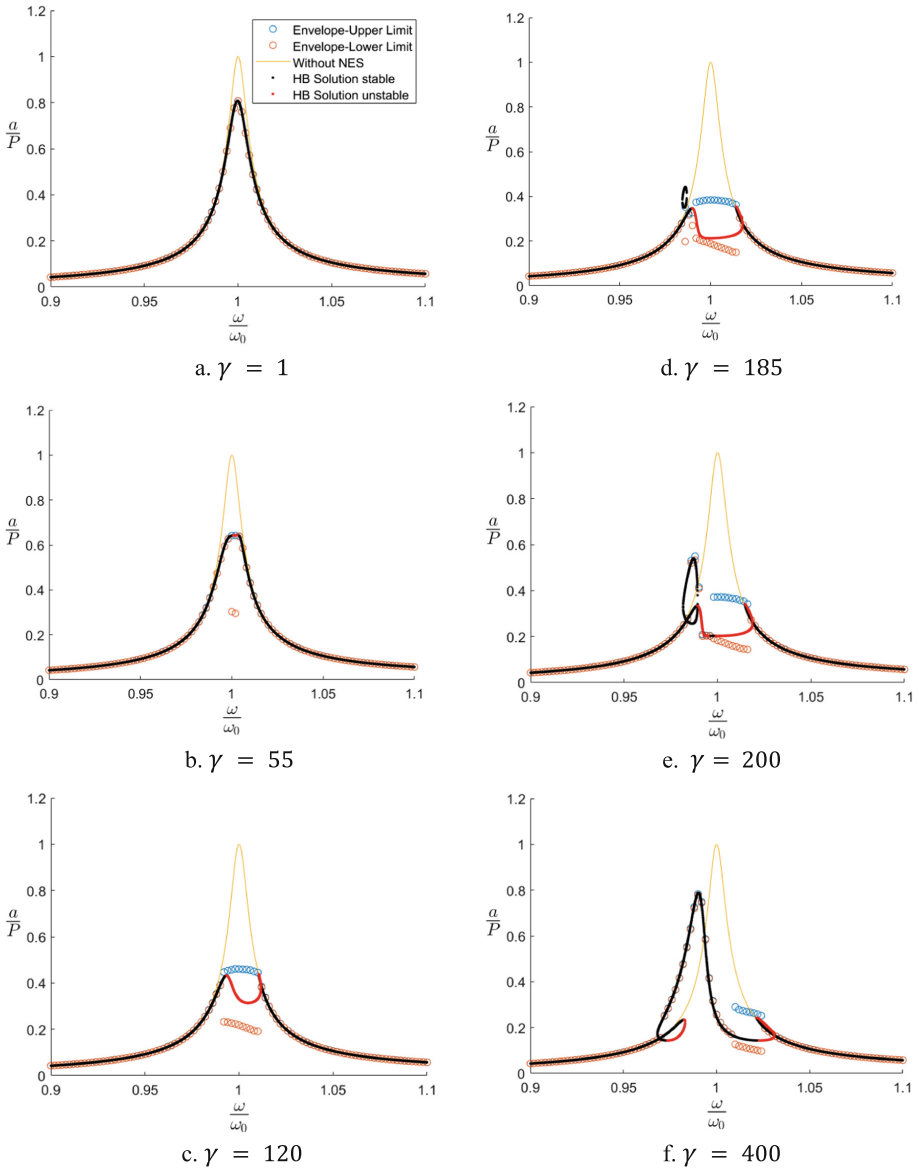

Fig. 4. Frequency response of the primary system for various k_{na} for NES with hardening stiffness

3.2 Primary System with Softening NES

The arctangent function of the softening stiffness force has two main factors namely γ controlling the ceiling of the restoring force, and k_s controlling the degree of nonlinearity of the stiffness function. Figure 5 below shows the influence of these factors. Table 2 details the input values chosen for analysis.

Table 2. Parameter values for primary system with softening NES.

Parameter	Value
ξ_{na}	0.25
ξ	1
γ	0.01–1
μ	0.01
ω_0[rad/s]	1
k_s	10–60
$e[m]$	0.001

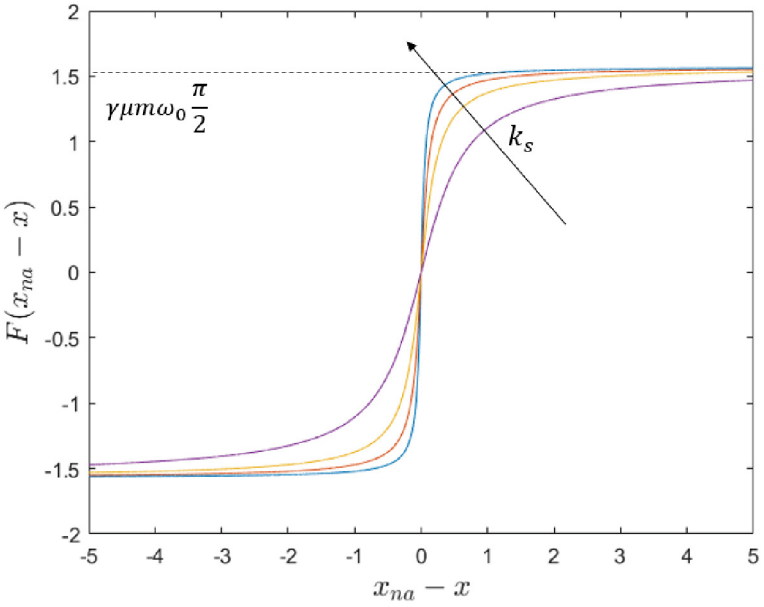

Fig. 5. Arctangent function with factors C and γ

In the case of softening stiffness, both γ and k_s are varied as shown in Fig. 6 below. In general for all values of γ and k_s, the numerical simulations agree well with the HB solution, except in the region of HB-unstable. This is because of the previously mentioned Neimark-Sacker bifurcations. For a given k_s, there is an optimal γ above and below which the response of the primary system approaches to that of without having the NES (see Fig. 6a–c). This is because changing γ also changes the slope of the initial, approximately-linear region of the arctan function. Thus, it can also be the case that the response purely lies within the quasi-linear region of the stiffness function.

Changing k_s also causes the same effect, but with the additon of changing the non-linearity of the function. Therefore, it causes the typically nonlinear behaviour of having

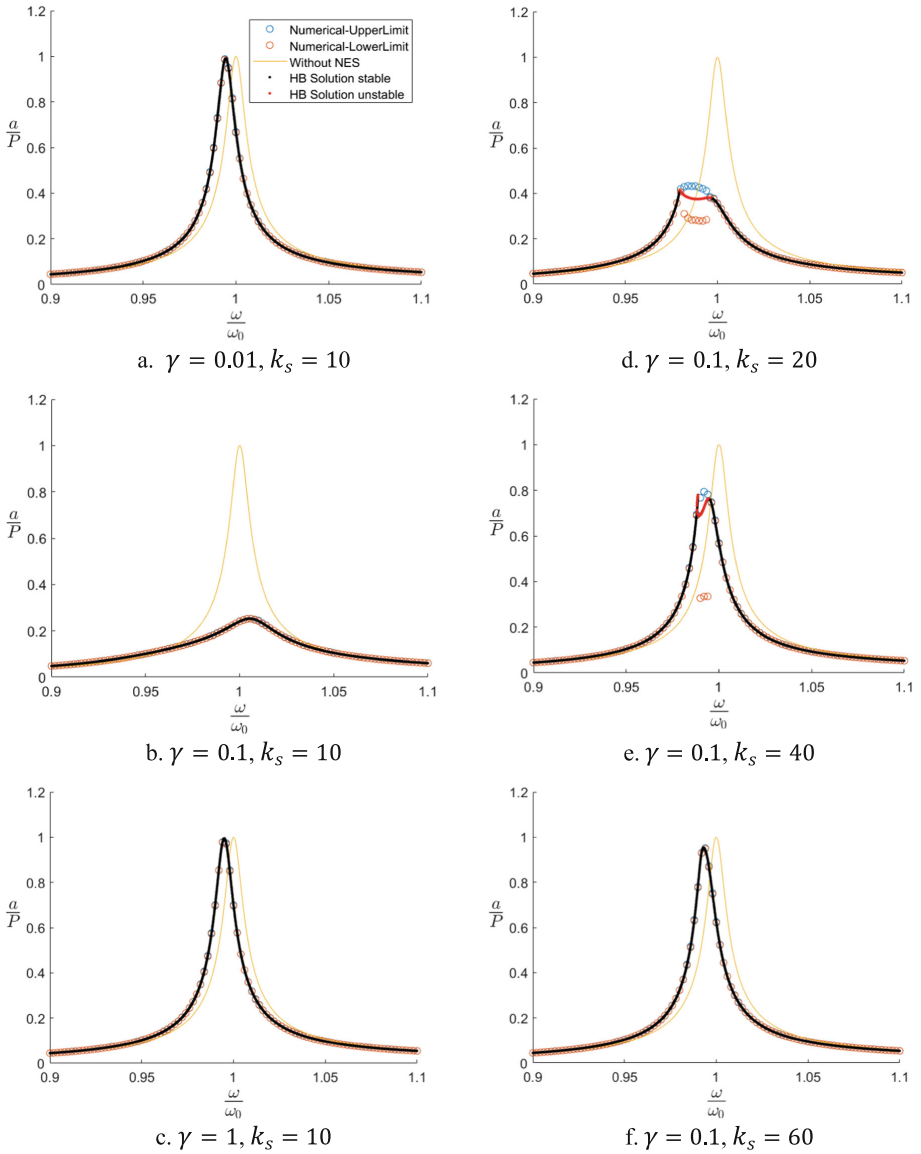

Fig. 6. Frequency response of the primary system for various γ and C for NES with softening stiffness

bifurcations and regions of quasi-periodic responses. In this case, the response displacement stays below the limit where the stiffness force becomes constant (see Fig. 5), and thus linearity is still prominent. Thus at higher k_s the linear part of the stiffness curve has shifted from its optimum. This explains the effect shown in Fig. 6d–f. Additionaly, the lack of IRCs should also be noted, as it is a significant advantage in terms of tuning.

As seen for hardening stiffness, the damping has no effect on the possible behaviour that can be observed and only affects the range of values where a behaviour is observed.

4 Comparison of Stiffness Characteristics

Both stiffness models are compared based for their vibration suppression capabilities and their behaviour qualities for the primary system given in Tables 1 and 2. It should be noted that bifurcations and unstable regions (i.e. the typically nonlinear behaviour) arise only when the response goes through a highly-nonlinear region in the stiffness function. This can be the case when there is either high forcing (via eccentricity e) or light damping or when the nonlinearity constants are high. Since there is only a single factor to control in hardening stiffness (i.e. γ), which decides its degree of nonlinearity, increasing γ to lower the response makes this aforementioned behaviour unavoidable. This is in contrast to softening stiffness, where the nonlinearity factor k_s can be modified separately from saturation factor γ. Additionally, from the parametric analysis it is evident that for the given range of values IRCs are absent in the system with the softening stiffness, which is greatly advantageous for tuning applications.

The comparison with optimal values is visualized in Fig. 7. Here the HB solutions and the upper envelope values from numerical simulation are presented for both cases. Based on the parametric analysis, for hardening stiffness, increasing γ leads to lower response at primary system resonance. However, $\gamma = 183$ is chosen as the optimal value for hardening stiffness, as higher values lead to IRCs of high peak response. Similarly,

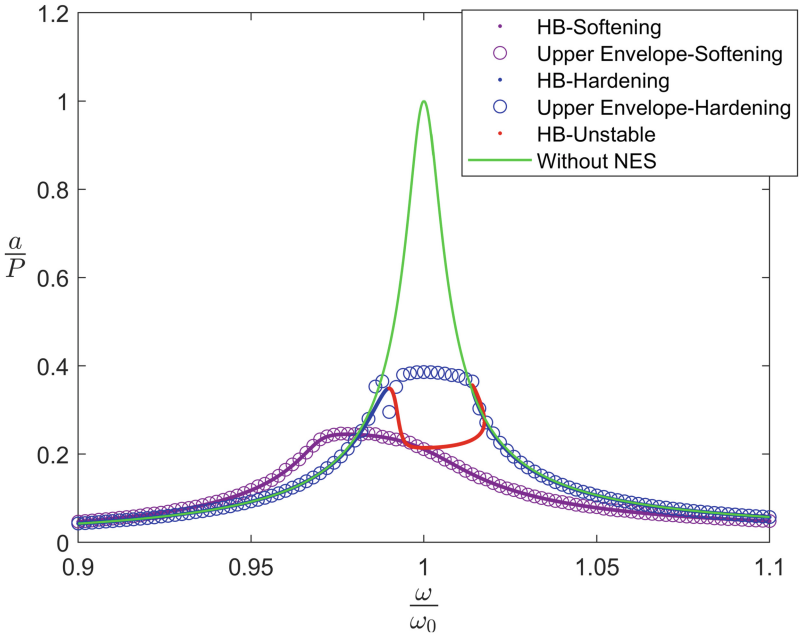

Fig. 7. Optimal response curve for both hardening and softening NES.

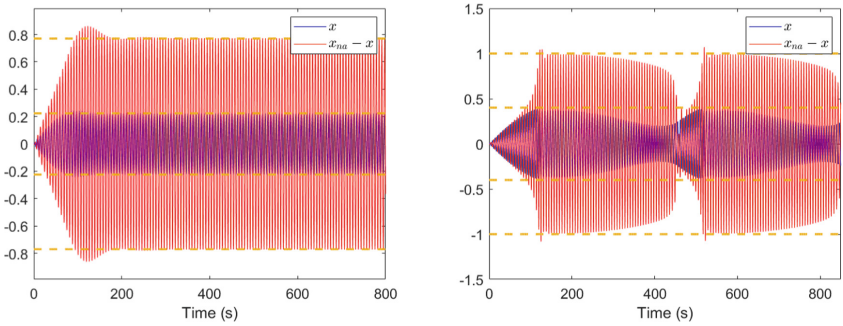

Fig. 8. Comparison of scaled time responses at $\left(\frac{\omega}{\omega_0}\right) = 1$, for both softening (a) and hardening (b) NES attachment.

for softening stiffness an optimal γ and k_s is found based on its response reduction. The value of k_s is also selected so as to include a reasonable degree of nonlinearity. Hence, $\gamma = 0.1$ and $k_s = 14$ is taken as the optimum. A time simulation at $\left(\frac{\omega}{\omega_0}\right) = 1$ is shown in Fig. 8.

The response plot above shows a clear advantage for the softening stiffness. It should be noted that at the instability regions in the HB-hardening, the numerically calculated envelope limits are better estimates of the response magnitude. The NES with softening stiffness is able to achieve 79% response reduction at the primary system resonance when compared to 62% with the hardening NES. This can also be verified from the time simulation in Fig. 8. Furthermore, the amplitude modulation of the quasi-periodic response for the hardening NES could also be considered undesirable. For modelling purposes, the optimized stiffness function can be used to obtain the nonlinear profile $f(x)$ for the realization shown in Appendix A.

5 Conclusion

A simplified Jeffcott rotor model coupled to an NES with stiffness nonlinearity is explored in this paper for its feasibility, primarily through the Harmonic Balancing method. The HB method has been successfully implemented in this regard and validated using response envelopes from time simulations; save for the regions detected by HB as unstable, where a quasi-periodic response is observed. An intuitive comparison between hardening and softening stiffness of the NES has been made based on their behaviour and their vibration absorption capability. It has been found that the softening NES has a distinct advantage over the conventional hardening NES, both in terms of avoiding IRCs and in terms of optimal response attenuation. The current model relies on the simplification that the rotor system is symmetric, removing the cross-coupling of coordinates. In the future, a more generalized (non-symmetric) rotordynamic system will be considered, with inclusion of coupling and gyroscopic effects. The robustness of the NES, i.e. usefulness of de-tuning, would also be explored in detail.

Appendix A: Realization of Stiffness Nonlinearity

This section details the method used in [3] to create nonlinear stiffness for the NES attachment. Here the NES is attached to a linear spring with a rolling element on the other side. The rolling element is made to follow a nonlinear guided path designed according to the optimized parameters of the nonlinear stiffness function. Figure 9 below shows the principle.

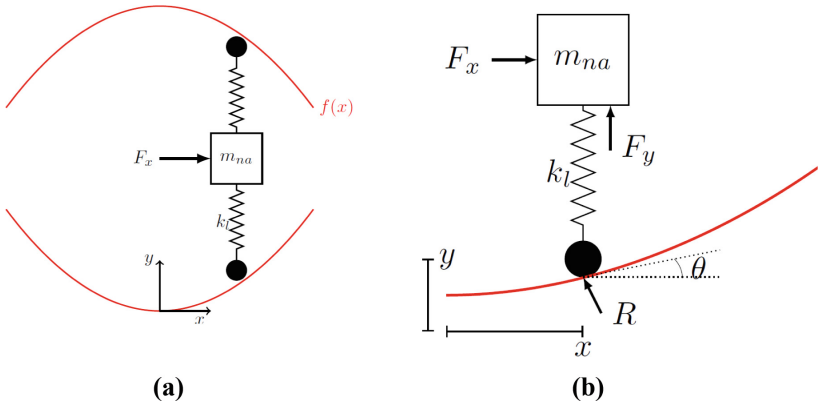

Fig. 9. Realization of custom nonlinear stiffness using a nonlinear profile $f(x)$ (a) with its force balance (b) [3]

The NES mass m_{na}, with motion along x, is attached to a linear spring with spring constant k_l, which is compressed according to a nonlinear profile $f(x)$. The reaction forces F_x and F_y are defined as follows:

$$F_x = 2Rsin(\theta), \quad F_y = Rcos(\theta), \tag{43}$$

$$\Rightarrow F_x = 2F_y tan(\theta), \tag{44}$$

where $tan(\theta) = \frac{\partial f(x)}{\partial x}$ and $F_y = k_l f(x)$

The given stiffness function F_x will be equated according to Eq. (44) to obtain the profile $f(x)$.

References

1. Friswell, M.I., et al.: Dynamics of Rotating Machines. Cambridge University Press (2010). https://doi.org/10.1017/CBO9780511780509
2. Genta, G.: Dynamics of Rotating Systems. Springer US, New York, NY (2005)
3. Dekemele, K.: Performance measures for nonlinear energy sinks in mitigating single and multi-mode vibrations: theory, simulation and implementation. Diss. Ghent University (2021)
4. Den, H., Pieter, J.: Mechanical Vibrations. Courier Corporation (1985)

5. Kuether, R.J., et al.: Nonlinear normal modes, modal interactions and isolated resonance curves. J. Sound Vib. **351**, 299–310 (2015). https://doi.org/10.1016/j.jsv.2015.04.035
6. Tehrani, G.G., Dardel, M., Pashaei, M.H.: Passive vibration absorbers for vibration reduction in the multi-bladed rotor with rotor and stator contact. Acta Mech. **231**(2), 597–623 (2019)
7. Bab, S., et al.: Vibration attenuation of a continuous rotor-blisk-journal bearing system employing smooth nonlinear energy sinks. Mech. Syst. Signal Process. **84**, 128–157 (2017)
8. Yao, H., Zheng, D., Wen, B.: Magnetic nonlinear energy sink for vibration attenuation of unbalanced rotor system. Shock Vib. **2017**, 1–15 (2017)
9. Zou, D., et al.: A device capable of customizing nonlinear forces for vibration energy harvesting, vibration isolation, and nonlinear energy sink. Mech. Syst. Signal Process. **147**, 107101 (2021)
10. Dekemele, K., Habib, G.: Inverted resonance capture cascade: modal interactions of a nonlinear energy sink with softening stiffness. Nonlinear Dyn. **111**, 9839–9861 (2023)
11. Krack, M., Gross, J.: Harmonic Balance for Nonlinear Vibration Problems, vol. 1. Springer International Publishing, Cham (2019)
12. Dekemele, K., Habib, G., Loccufier, M.: The periodically extended stiffness nonlinear energy sink. Mech. Syst. Signal Process. **169**, 108706 (2022)
13. Dekemele, K., Habib, G., Loccufier, M.: Vibration mitigation with a nonlinear energy sink having periodically extended stiffness. In: ISMA: International Conference on Noise and Vibration Engineering (2022)
14. Smirnov, V.V., Manevitch, L.I.: Complex envelope variable approximation in nonlinear dynamics. Rus. J. Nonlin. Dyn. **16**(3), 491–515 (2020)
15. Kuznetsov, Y.A., Sacker, R.J.: Neimark-Sacker bifurcation. Scholarpedia **3**(5), 1845 (2008)